PHILOSOPHICAL TRANSACTIONS OF THE ROYAL SOCIETY A MATHEMATICAL, PHYSICAL & ENGINEERING SCIENCES

Resolution of Cellular Structures by NMR Microscopy at 11.7 T [and Discussion]

R. W. Bowtell, G. D. Brown, P. M. Glover, M. McJury, P. Mansfield, J. M. Pope, R. E. Ratcliffe, J. Waterton and W. E. Timms

Phil. Trans. R. Soc. Lond. A 1990 **333**, 457-467
doi: 10.1098/rsta.1990.0173

Resolution of cellular structures by NMR microscopy at 11.7 T

By R. W. Bowtell, G. D. Brown, P. M. Glover, M. McJury and P. Mansfield

Department of Physics, University of Nottingham, University Park, Nottingham NG7 2RD, U.K.

An NMR microscope with an operating frequency of 500 MHz has been constructed. Using this instrument images showing cellular detail in plant systems have been generated. These have a best in-plane resolution of 4.5 μm and a slice thickness of 100 μm. Many features of these images can be interpreted as the effects of local magnetic susceptibility differences inside the sample.

1. Introduction

Although the idea of NMR microscopy was suggested in some of the earliest papers on NMR imaging (Mansfield & Grannell 1973, 1975), it is only in recent years that improvements in magnet technology have allowed its practical realization (see, for example, Aguayo *et al.* 1986; Cho *et al.* 1988). At currently available magnetic field strengths the necessity of producing images with an adequate signal-to-noise ratio (SNR) in a reasonable time poses a lower bound on the attainable resolution of the order of several micrometres. Optical microscopy can of course yield resolution an order of magnitude better than this, but its use requires destructive preparation of the sample. NMR microscopy on the other hand can be applied to living systems and in particular it can be used to investigate the spatial and temporal variation of the concentration and the state of water *in vivo* at cellular level. We have recently constructed an NMR microscope which has allowed us to produce images with an in plane resolution of 4.5 μm and slice thickness 100 μm showing cellular detail in plant systems. The instrumentation, which includes specially designed actively screened gradient coils, is described in §2.

For several reasons plant stems are well suited to investigation by NMR microscopy. Firstly, no special apparatus is required to keep stems viable; secondly, their constituent cells are typically much larger than those found in animal systems; and finally, the stem structure varies slowly along its length, so that gains in SNR can be made by imaging with a slice width considerably larger than the in-plane resolution without introducing loss of detail due to partial volume effects. We have investigated the stems of several different types of vascular plants using NMR microscopy concentrating mainly on those of the geranium (*Pelargonium graveolens*). The results of this work are presented in §3. These indicate that many of the features in high-resolution images of plant stems obtained at high magnetic field strengths are caused by the small local differences in magnetic susceptibility which occur inside the sample. Such differences produce local changes in the magnetic field which may distort the image (Ludeke *et al.* 1985; Callaghan 1990). The major effect in our

images, is, however, the loss of signal caused by the diffusion of water molecules in the very large magnetic field gradients which can occur close to the interfaces between regions of different magnetic susceptibility (Case *et al.* 1987). In the geranium the main sources of these gradients are the small intercellular air spaces which permeate some tissues of the stem. An analysis of these effects including computer simulations is also presented in §3.

2. Instrumentation and methods

The NMR microscope is based around an 11.7 T, 89 mm bore superconductive magnet. This gives a proton resonant frequency of 500 MHz. Inside the magnet shim and gradient coils reduce the diameter of the usable bore to 30 mm.

The ability to generate large magnetic field gradients is a prerequisite for the implementation of NMR microscopy. Large gradients are required firstly to limit the broadening of the lineshape, which is caused by diffusion of spins in the presence of the read gradient during signal acquisition (Callaghan & Eccles 1988). Secondly, they are needed to reduce the attenuation of the signal which occurs before acquisition through diffusion in the presence of the field gradients used in phase encoding and slice selection. In general to reap the benefits of using large gradients it is necessary to be able to rapidly switch them on and off.

These requirements are fulfilled in our experiments by the use of a specially designed screened gradient coil set. The x, y and z gradient coils of this set have efficiencies of 23, 20 and 14 $\mathrm{mT\,m^{-1}\,A^{-1}}$ and inductances of 30, 40 and 20 μH respectively. The transverse gradients are produced by modified Golay coils, whose saddle spacings have been altered to allow for the presence of the screening coils. The z gradient coil was designed using the target field approach (Turner 1986), with the target field chosen so as to minimize the power dissipation in the coil, while approximating a linear field gradient over an adequate volume. Incorporation of active magnetic screening (Mansfield & Chapman 1986) severely reduces the problems of eddy currents, normally present when gradient coils are switched inside superconductive magnets. This is because the screened coils produce a field attenuated by two orders of magnitude relative to that from the inner coil alone, at a distance of 40 mm from the axis of the coil set.

Construction of distributed arc gradient coils on small cylindrical formers poses some problems. Winding small coils by hand is usually not sufficiently accurate, while the use of etching techniques (see, for example, Bowtell & Mansfield 1990) although accurate, makes it difficult to produce a large enough current carrying cross section to limit the power dissipation in the coils. We have overcome these problems by using a home-built computer-controlled gradient coil cutter. This uses two stepper motors to give independent axial and azimuthal movements with respective accuracies of 0.3° and 0.01 mm. Coils are constructed with this tool by cutting grooves in a Tufnol former into which wires can then be accurately cemented.

The radio frequency (RF) coil used for imaging plant stems is a simple six-turn solenoid with an inner diameter of 1.5 mm. This mounts onto an RF stage containing tuning and matching circuitry, a stripline isolator and the preamplifier (Glover *et al.* 1989). In the imaging experiments sections of stem which approximately fitted the RF coil were cut from the plant. Both cut ends were sealed with wax before the section was placed in the coil. This ensured that the stem cells remained turgid throughout the experiment.

PHILOSOPHICAL TRANSACTIONS OF THE ROYAL SOCIETY A MATHEMATICAL, PHYSICAL & ENGINEERING SCIENCES

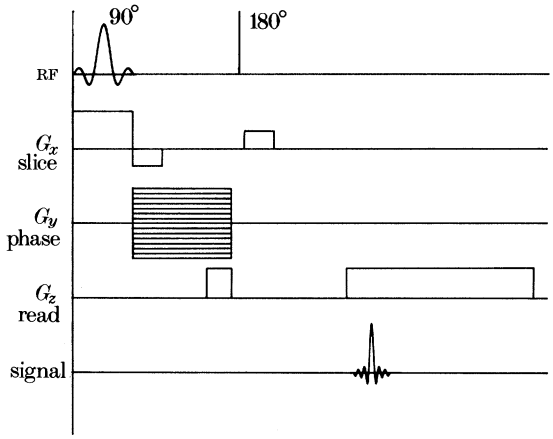

Figure 1. The half-Fourier spin warp sequence used for imaging.

The imaging sequence currently used is shown in figure 1. It is a standard half-Fourier spin warp imaging sequence (Edelstein *et al.* 1980), incorporating a non-selective 180° refocusing pulse. In high-resolution imaging considerable gains in SNR can be made by adopting the half-Fourier technique in which data spanning only half of k-space, in the direction defined by the read gradient, is gathered. This is because with this sequence the attenuation of the echo amplitude caused by diffusion in the read gradient is much less than that which occurs when both halves of k-space must be spanned (Cho *et al.* 1988). This effect is demonstrated in figure 2. Figure 2*a* shows an image of a tube of diameter 900 μm containing doped water, acquired using the sequence of figure 1. The in-plane resolution is 9 μm and the slice thickness is 200 μm. Figure 2*b* is an image of the same object generated using the same gradient strengths and bandwidth, but using a sequence in which data spanning both halves of k-space are gathered. The substantially lower SNR in the image of figure 2*b* can be clearly seen.

3. Results

Figure 3 shows a 256×256 NMR image of a 1 mm diameter geranium petiole. This image has an in plane resolution of 6.5 μm and a slice thickness 100 μm. An annotated optical micrograph obtained after sectioning and staining of the same petiole is shown in figure 4. From this figure it can be seen that most of the central region of the petiole is parenchyma. The cells of this tissue are relatively large with a width of between 40 and 120 μm, and are highly vacuolated. They are also quite loosely packed and intercellular air spaces with a maximum size of 10 μm are formed at their junctions. In the centre of the stem a vascular bundle of phloem and xylem vessels is found. The cells in these tissues are less than 15 μm in width and are tightly packed together. Vascular bundles also appear just inside the fibrous sheath which is formed around the parenchyma. The cells of this tissue are small (10–15 μm) and are held together by a hydrated pectinaceous medium which fills all the intercellular spaces. Outside this sheath the cells of the cortex are similar to those of the parenchyma, but are smaller (10–50 μm) and there is a higher density of intercellular air spaces in this region. Finally, the exterior of the stem is bounded by the epidermis which is made up of a single layer of small cells.

PHILOSOPHICAL TRANSACTIONS OF THE ROYAL SOCIETY A MATHEMATICAL, PHYSICAL & ENGINEERING SCIENCES

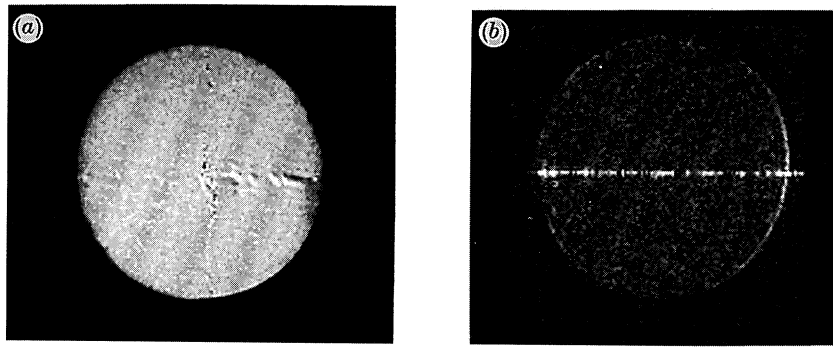

Figure 2. (*a*) NMR image of a 900 μm diameter tube containing doped water, obtained using the imaging sequence of figure 1. The resolution is 9 μm and the slice thickness 200 μm. (*b*) Image of the same sample obtained using a sequence in which both sides of *k*-space are sampled. The resolution, slice thickness, gradient strength, bandwidth and imaging time were the same as in (*a*).

Figure 3

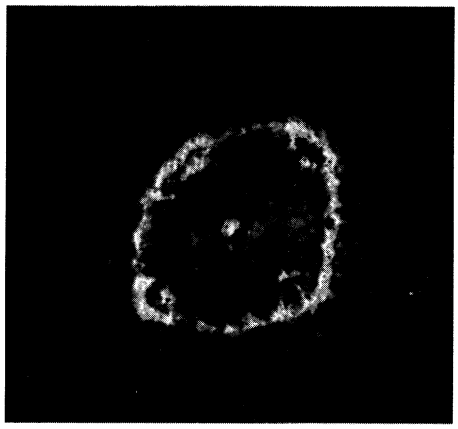

Figure 4

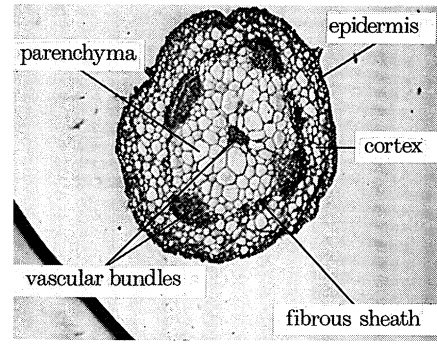

Figure 3. 256 × 256 NMR image of a geranium stem. The in-plane resolution is 6.5 μm and the slice thickness is 100 μm.

Figure 4. Annotated optical micrograph of a section of the same geranium stem as seen in figure 3.

Comparison of figures 3 and 4 indicates that the brightest features in the NMR image of the geranium petiole are produced by the fibrous sheath and the vascular bundles, both of which are made up of small closely packed cells. Single parenchymatus cells can be discerned in the central region of the image, but their apparent size is less than would be expected from the optical micrograph. In this region there are dark areas which do not simply correspond with any real structure in the stem. Only a few cells of the cortex appear in the image, but it is just possible to make out the outline of the epidermis. These features are broadly repeated in the many images of geranium petioles of various sizes which have been generated, although in some cases the xylem may appear dark if water has leaked out of it when the stem was cut. Figure 5 shows a 4.5 μm resolution image of a geranium stem, with a slice thickness of 100 μm. This image was obtained after the averaging of 16 data-sets giving an imaging time of *ca.* 70 min.

Much of the appearance of the NMR images of petioles can be explained by

PHILOSOPHICAL TRANSACTIONS OF THE ROYAL SOCIETY A MATHEMATICAL, PHYSICAL & ENGINEERING SCIENCES

Figure 5

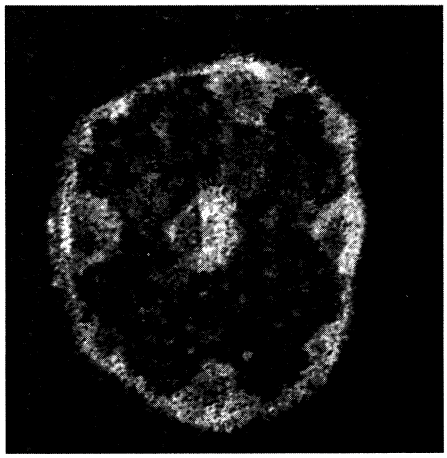

Figure 6

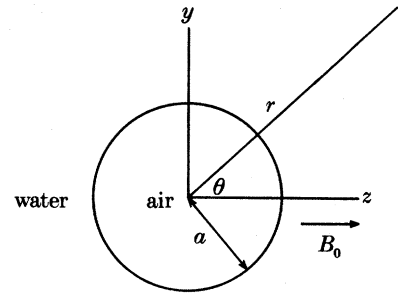

Figure 5. NMR image of a geranium stem with an in-plane resolution of 4.5 μm and slice thickness 100 μm.

Figure 6. Geometry of a simple model of the intercellular air spaces.

consideration of the effects of magnetic susceptibility differences between cells and the intercellular air spaces. Highly vacuolated cells can be expected to have a volume susceptibility approximately the same as that of free water, which is different to that of air by an amount $\Delta\chi = -9\times10^{-6}$. At 11.7 T in bulk media this would correspond to a difference in the frequency of proton resonance of 4.5 kHz. Of course the variation of the magnetic field inside an inhomogeneous sample depends on the shape of the boundaries between materials of different magnetic susceptibility and their orientation relative to the applied magnetic field. The intercellular air spaces in the geranium are, like the cells, much longer than they are wide. A single air space may therefore be simply modelled as a long cylinder, which because of the sample orientation will have its axis perpendicular to the applied field. This geometry is shown in figure 6. It is well known that the extra external field produced by a cylindrical cavity of radius a is given by

$$\Delta B_0 = -(B_0\,\Delta\chi a^2\cos 2\theta)/2r^2, \tag{1}$$

where the applied magnetic field B_0 is in the z direction, θ and r are defined in figure 6, and it is assumed that the magnetic susceptibilities of both materials are much less than one (see, for example, Ludeke *et al.* 1985). With the spin warp imaging technique of figure 1, the presence of the 180° pulse means that at the start of data signal sampling there is no accumulated phase due to the evolution of spins in the extra field ΔB_0. Thus there is no image distortion in the direction of the phase encode gradient. However, the presence of the extra field during signal acquisition causes spins at position (y, z) to appear in the image at position $(y, z+\Delta B_0(y,z)/G)$ (Callaghan 1990), where G is the read gradient strength.

The distortion caused by this variable shift in the direction of the read gradient can be simply simulated by computer. This is done by breaking up the region around the cavity into an array of equally spaced points, and then creating an image by adding an equal contribution from each point into the image at a pixel position specified by the point coordinates and the extra field calculated from equation (1). Figure 7*a*

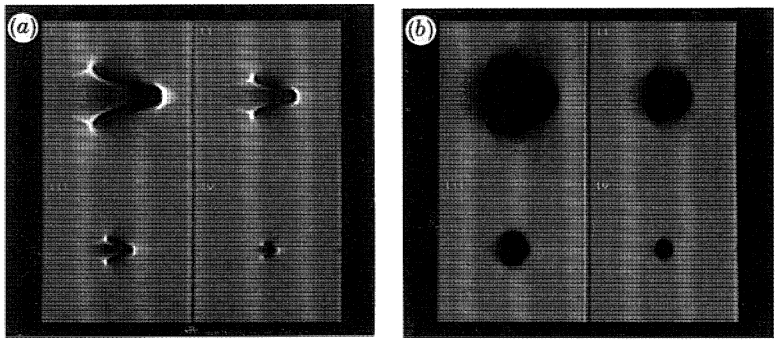

Figure 7. Simulated NMR images of air cavities in water. The resolution is 6 μm, the gradient strength is 0.5 T m^{-1} and $\tau = 5.5$ ms. The cavity diameters are (i) 100 μm, (ii) 50 μm, (iii) 25 μm and (iv) 10 μm. In (*a*) only the distorting effect of the extra field ΔB_0 is included. In (*b*) the effect of diffusion in the gradient G_s is also incorporated.

shows the results of carrying out this procedure in the situation where the read gradient and main field directions are the same. The read gradient was set at 0.5 T m^{-1}, the main field as 11.7 T and the pixel spacing as 6 μm. The diameter of the air gaps vary from 100 μm in image (i) down to 10 μm in image (iv). The considerable distortion is clearly seen, with the θ variation of ΔB_0 giving rise to the characteristic 'spearhead' shape described elsewhere (Ludeke *et al.* 1985).

The extra field ΔB_0 varies spatially so diffusion of spins in its presence causes an irreversible dephasing of any transverse magnetization. Hence a second effect in the images is a loss of signal close to the cavity. Differentiation of (1) indicates that the magnitude of the gradient of ΔB_0 is independent of θ and given by

$$G_s = \Delta\chi B_0 a^2/r^3. \tag{2}$$

For a cavity of diameter *ca.* 10 μm as is found in the geranium stems the maximum gradient is therefore *ca.* 20 T m^{-1}. This is substantially larger than any applied field gradient in our imaging experiment. Neglecting the effect of local variation in the gradient, the attenuation of the signal in the image produced by diffusion in a gradient G_s is expected to be as $\exp(-\frac{2}{3}(\gamma G_s)^2 D\tau^3)$, where D is the self diffusion coefficient and τ the time between 90° and 180° pulses. In our experiment $\tau \approx 5.5$ ms, so for the 10 μm cavity this means that even at a distance of 21 μm from the cavity centre where the maximum distortion is less than one pixel spacing the signal is attenuated to 30% of its expected value. So for small cavities the destruction of the signal by diffusion in the spatially varying field ΔB_0 is a more important effect than the image distortion. This conclusion is borne out by the simulations of figure 7*b*. These have been made using the same parameters as in figure 7*a*, but the effect of the signal attenuation due to diffusion has been incorporated. It can be seen that in the image of the 10 μm cavity diffusion produces a dark almost circular region around the cavity, whereas in those of the larger cavities the 'spearhead' pattern still partly remains.

These effects can also be simulated experimentally using a model system of glass fibres in water. Figure 8*a* shows four 30 μm resolution images of glass fibres immersed in water inside a tube of diameter 3 mm. The fibre diameters vary from 700 μm in image (i) down to 100 μm in image (iv). The gradient strength used was 120 mT m^{-1}, the bandwidth 20 kHz and the time τ was 5.5 ms. The distortions in

PHILOSOPHICAL TRANSACTIONS OF THE ROYAL SOCIETY A MATHEMATICAL, PHYSICAL & ENGINEERING SCIENCES

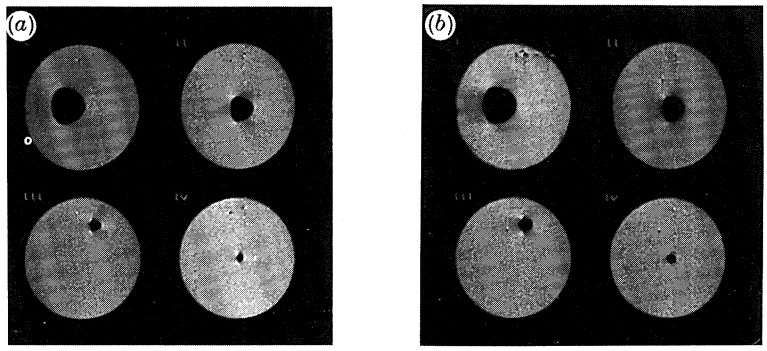

Figure 8. 30 μm resolution images of glass fibres in water in a tube of diameter 3 mm. The fibre diameters are (i) 700 μm, (ii) 400 μm, (iii) 200 μm, and (iv) 100 μm. The gradient strength used was 120 mT m^{-1} and the bandwidth 20 kHz. In (*a*) $\tau = 5.5$ ms and in (*b*) $\tau = 15$ ms.

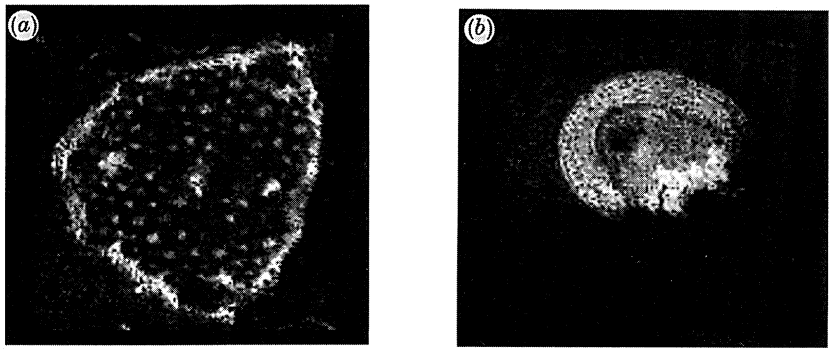

Figure 9. (*a*) 7.5 μm resolution NMR image of an intact geranium stem. (*b*) One quarter of the same stem after sectioning and soaking in water for 15 min.

these images are similar in type to those of figure 7*a*; however, the smaller difference $\Delta\chi$ between the susceptibilities of water and the glass used, makes them less severe. Figure 8*b* shows images of the same samples, but here at the time τ has been extended to 15 ms, thus increasing the diffusion weighting. The image of the 700 μm fibre is not greatly changed, but as the fibre diameter is decreased the effect of diffusion becomes more important. In the image of the 100 μm fibre the attenuation of the signal due to diffusion produces a nearly circular dark region round the rod.

The effects outlined above can be used to largely explain the appearance of images of geranium and other plant stems. In the cortex the high density of intercellular air spaces and the small cell size mean that there are large field gradients throughout this region. With our imaging parameters diffusion-dependent dephasing of the magnetization therefore essentially destroys all the NMR signal from cortical cells before signal acquisition, so they do not appear in an image. In the central parenchyma there is a lower density of air spaces, so parenchymatus cells are present in the images. However, diffusion in regions close to air gaps makes the cells appear smaller than they really are and gives rise to dark areas. The fibrous sheath and vascular bundles contain no air spaces and hence appear bright in the images. Confirmation that this explanation of the image appearance is broadly correct is obtained from figure 9. Figure 9*a* shows an image of an intact geranium stem. The in-plane resolution is 7.5 μm, the slice thickness 100 μm, and the imaging time was

PHILOSOPHICAL TRANSACTIONS OF THE ROYAL SOCIETY A MATHEMATICAL, PHYSICAL & ENGINEERING SCIENCES

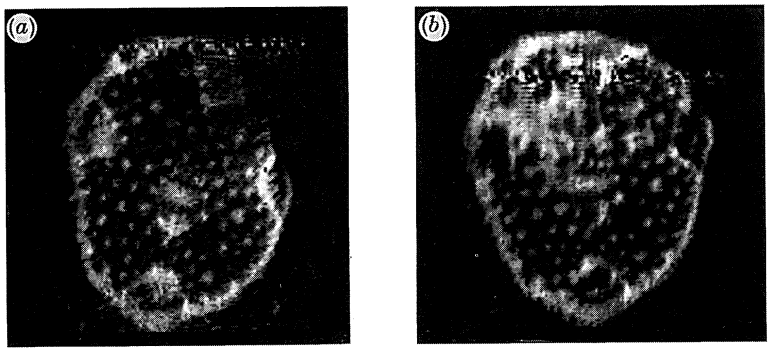

Figure 10. 7.5 μm resolution NMR image of a geranium stem before (*a*) and after (*b*) bruising.

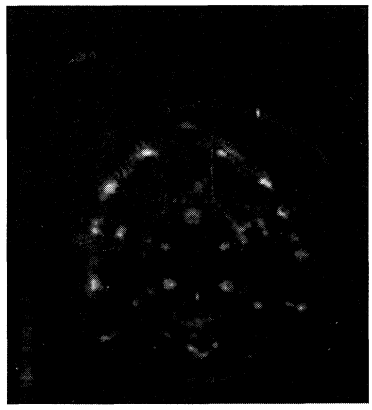

Figure 11. 10 μm resolution NMR image of a grass stem.

ca. 10 min. After imaging the stem was quartered longitudinally and soaked in water for 15 min. Figure 9*b* shows an image of one section of the soaked stem. In this image the cortex now appears relatively bright and layers of cells can be observed. The central parenchyma appears uniformly bright. This change of appearance occurs because water has infiltrated the intercellular air spaces thus eliminating susceptibility differences. The same changes are seen when D_2O is infused into an intact stem section. This behaviour makes NMR microscopy particularly sensitive to bruising in plant stems. Figure 10*a*, *b* shows a geranium stem before and after bruising. The bright regions which appear in figure 10*b* are produced by ruptured cells leaking water into the intercellular air spaces. This bruising was harder to detect in a corresponding optical micrograph, but a few broken cell walls could be seen.

Other plant stems imaged on our system have manifested the same sort of susceptibility effects. These have also been noted in images of the roots of the maize plant (Connelly *et al.* 1987). Figure 11 shows an image of a grass stem, with an in-plane resolution of 10 μm. The central region of the stem appears dark in the image because it contains a high density of intercellular air spaces, while the small tightly packed cells of the vascular bundles appear bright.

4. Conclusion

A specially constructed NMR microscope for use at 11.7 T, has been described and images showing cellular detail in vascular plant stems have been presented. Simple calculations and simulations indicate that much of the appearance of these images is a result of the loss of signal caused by diffusion in the local field gradients that surround intercellular air spaces. Elimination of these susceptibility effects would require the use of applied magnetic field gradients large enough to dominate the susceptibility induced gradients. These can be as large as 20 T m^{-1}, which is a gradient strength well beyond our present capability. Large applied gradients imply large bandwidths and an inevitable loss of SNR which can only be regained by going to coarser resolution or higher magnetic field. At present gradient strengths the local loss in signal around air spaces can however be used as a source of contrast, which allows discrimination of different tissues in a plant stem.

We thank the Royal Society Paul Instrument Fund for major support of the NMR microscope project. M.M. thanks the DENI for a research studentship.

References

Aguayo, J. B., Blackband, S. J., Schoeniger, J., Mattingly, M. A. & Hintermann, M. 1986 Nuclear magnetic resonance imaging of a single cell. *Nature, Lond.* **322**, 190–191.

Bowtell, R. W. & Mansfield, P. 1990 Screened coil designs for NMR imaging in magnets with transverse field geometry. *Meas. Sci. Technol.* **1**, 431–439.

Callaghan, P. T. 1990 Susceptibility-limited resolution in nuclear magnetic resonance microscopy. *J. magn. Reson.* **87**, 304–318.

Callaghan, P. T. & Eccles, C. D. 1988 Diffusion-limited resolution in nuclear magnetic resonance microscopy. *J. magn. Reson.* **78**, 1–8.

Case, T. A., Durney, C. H., Ailion, D. C., Cutillo, A. G. & Morris, A. H. 1987 A mathematical model of diamagnetic line broadening in lung tissue and similar heterogeneous systems: calculations and measurements. *J. magn. Reson.* **73**, 304–314.

Cho, Z. H., Ahn, C. B., Juh, S. C., Lee, H. K., Jacobs, R. E., Lee, S., Yi, J. H. & Jo, J. M. 1988 Nuclear magnetic resonance microscopy with 4 μm resolution: Theoretical study and experimental results. 1988 *Med. Phys.* **15**, 815–824.

Connelly, A., Lohman, J. A. B., Loughman, B. C., Quiqampoix, H. & Ratcliffe, R. G. 1987 High resolution imaging of plant tissues by NMR. *J. exp. Bot.* **38**, 1713–1723.

Edelstein, W. A., Hutchison, J. M. S., Johnson, G. & Redpath, T. 1980 Spin warp NMR imaging and applications to human whole-body imaging. *Phys. med. Biol.* **25**, 751–756.

Glover, P., Bowtell, R., Harvey, P., McJury, M., Brown, G. & Mansfield, P. 1989 A high resolution NMR microscope for use at 11.7 T. Abstracts, 8th Annual Meeting Society Magnetic Resonance in Medicine, p. 285.

Ludeke, K. M., Roschmann, P. & Tischler, R. 1985 Susceptibility artefacts in NMR imaging. *Magn. Res. Imaging.* **3**, 329–343.

Mansfield, P. & Chapman, B. 1986 Active magnetic screening of gradient coils in NMR imaging. *J. magn. Reson.* **66**, 573–576.

Mansfield, P. & Grannell, P. K. 1973 NMR 'diffraction' in solids? *J. Phys.* C **6**, L422–426.

Mansfield, P. & Grannell, P. K. 1975 'Diffraction' and microscopy in solids and liquids by NMR. 1975 *Phys. Rev.* B **12**, 3618–3634.

Turner, R. 1986 A target field approach to optimal coil design. *J. Phys.* D **19**, L147–L151.

PHILOSOPHICAL TRANSACTIONS OF THE ROYAL SOCIETY A MATHEMATICAL, PHYSICAL & ENGINEERING SCIENCES

Discussion

J. M. Pope (*University of New South Wales, Australia*). The images Dr Bowtell showed were of cut pelargonium stems. Cutting may allow additional air into the intercellular spaces. Has he imaged any intact, growing plants and does he observe differences when the items are not cut before imaging?

R. W. Bowtell. We have not as yet imaged any intact growing plants, but hope to do so in the near future. Other investigators who have looked at intact geranium stems by using a solenoidal RF coil have found a similar lowering of intensity in the central parenchyma and cortex which they were unable to fully explain in terms of T_1 effects (Brown *et al.* 1988). The intercellular air spaces which are involved in respiration are certainly present in the intact stem. In our experiments a 1–2 cm long stem section is excised from the plant, before imaging. This means that the cut ends are relatively far from the imaged region so the cutting process would be expected to have little effect on the size of intercellular air spaces in the central slice.

R. E. Ratcliffe (*Oxford University, U.K.*). (1) We observed the severe attenuation of the image intensity that occurs in root tissues several years ago and attributed this effect, as Dr Bowtell does in stems, to the presence of air spaces (Connelly *et al.* 1987). In a good physiological experiment it would be desirable to leave the air spaces, rather than to fill them by vacuum infiltration, and this raises the question as to whether it is possible to avoid the diffusion problem *in vivo* by modifying the parameters of the imaging experiment. (2) A point to bear in mind when extending the imaging method to plants concerns the difference in properties between animal and plant cells. It may be of general interest to note that Gd-(DTPA)$^{2-}$ can permeate cells (Quiquampoix *et al.* 1990) and so caution is needed in working with this contrast agent in plants.

R. W. Bowtell. (1) Theoretically, the diffusion problem may be avoided *in vivo* by increasing the gradient strength and shortening the echo time. Signal-to-noise losses incurred in this way can be alleviated by using repeated 180° RF pulses to generate a series of echoes which can then be co-added. However, with susceptibility induced gradients as large as 20 T m^{-1} this probably implies the use of unfeasibly large applied field gradients and bandwidth. A better solution which to some extent avoids this problem, may be to use 180° RF pulses interspersed in the acquisition of a single k-space line as was recently suggested by Callaghan (1990). (2) With onion epithelial cells and various undifferentiated cells in suspension we have found no evidence of Gd-DTPA crossing cell membranes into the cytoplasm or vacuole.

J. Waterton (*ICI Pharmaceuticals, U.K.*). I should like to point out that the air–space susceptibility problem has been solved in the case of *in vivo* spectroscopy. The solution is to use magic angle rotation. We have successfully used this technique in the case of wheat leaves. Obviously there are high gravitational forces involved, although these are less important for very small samples. Combination of magic angle rotation with imaging is clearly technically very challenging, but it seems to me it is possible in principle.

R. W. Bowtell. Images of solids rotating at the magic angle have been produced

(Cory *et al.* 1988). However, with the kind of intact biological samples which we would like to investigate by NMR microscopy, magic angle spinning is probably not a feasible approach.

W. E. TIMMS (*Oxford Instruments Ltd, U.K.*). When large pulsed gradients are applied to conductive samples in a high magnetic field there is the possibility of induced current flowing within the sample. These currents will experience a Lorentz force which may cause significant motion of the medium. Is there any evidence of this?

R. W. BOWTELL. We have to date found no evidence of the image blurring which might result from sample movement caused by Lorentz forces acting on induced currents. A simple analysis indicates that the magnitude of the current density induced in a cylindrical sample by a changing magnetic field depends on the product of the rate of change of field and the the sample radius (Mansfield & Morris 1982). So in NMR microscopy although relatively large values of dB/dt may occur inside the sample, its very small size probably limits the magnitude of induced currents and hence also associated Lorentz forces.

Additional references

Brown, J. M., Thomas, J. F., Cofer, G. P. & Johnson, G. A. 1988 Magnetic resonance microscopy of stem tissues of Pelargonium hortorum. *Bot. Gaz.* **149**, 253–259

Cory, D. G., van Os, J. W. M. & Veeman, W. S. 1988 NMR images of rotating solids. *J. magn. Reson.* **76**, 543–547.

Mansfield, P. & Morris, P. G. 1982 *Advances in magnetic resonance* (ed. J. S. Waugh). New York: Academic Press.

Quiquampoix, H., Ratcliffe, R. E., Ratkovic, S. & Vucinic, Z. 1990 *J. Biochem.* **38**, 265–275.

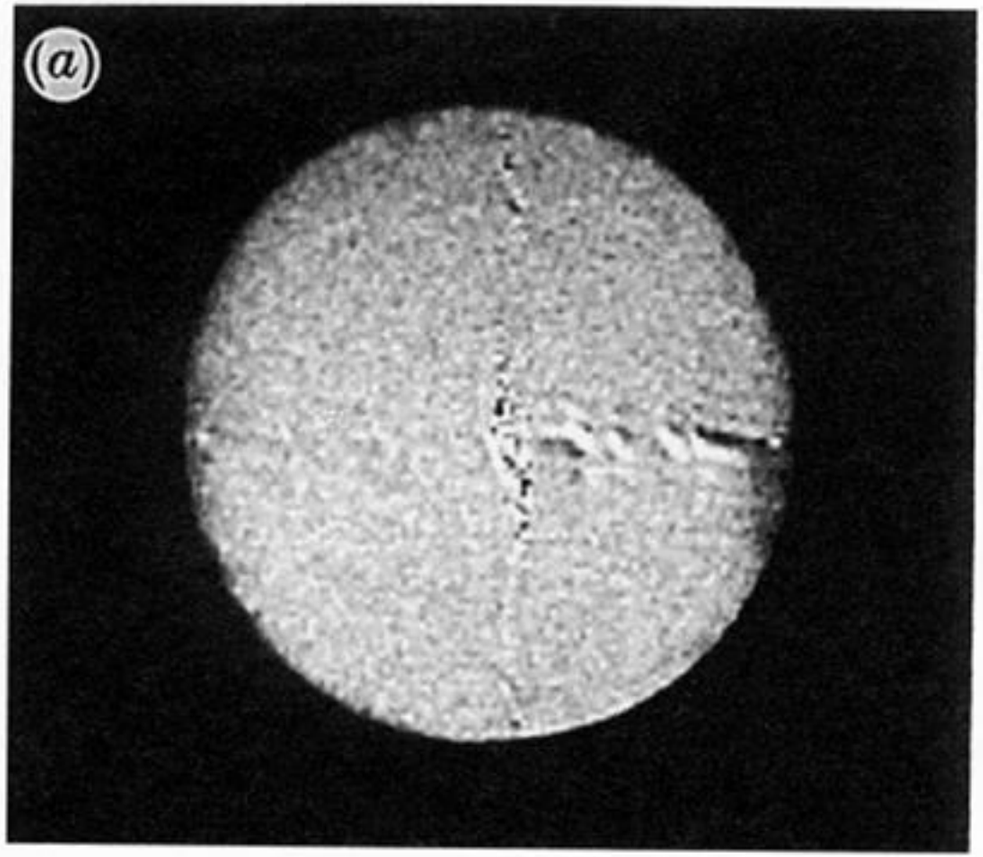

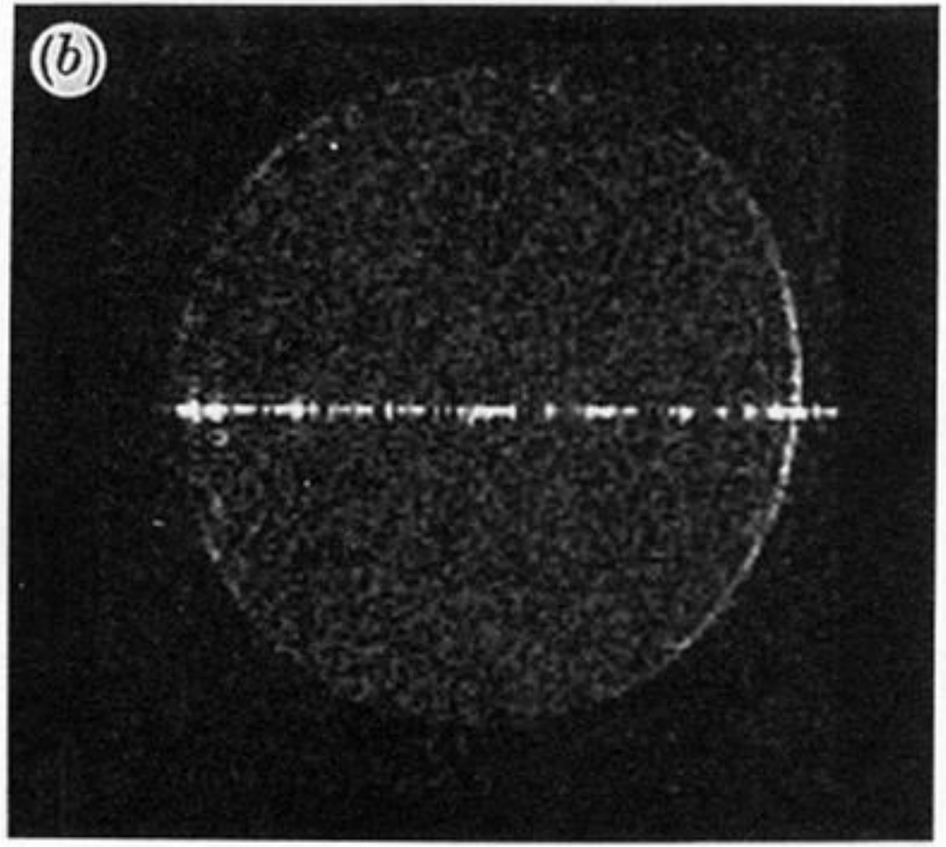

gure 2. (*a*) NMR image of a 900 μm diameter tube containing doped water, obtained using the aging sequence of figure 1. The resolution is 9 μm and the slice thickness 200 μm. (*b*) Image of e same sample obtained using a sequence in which both sides of *k*-space are sampled. The solution, slice thickness, gradient strength, bandwidth and imaging time were the same as in (*a*).

igure 3

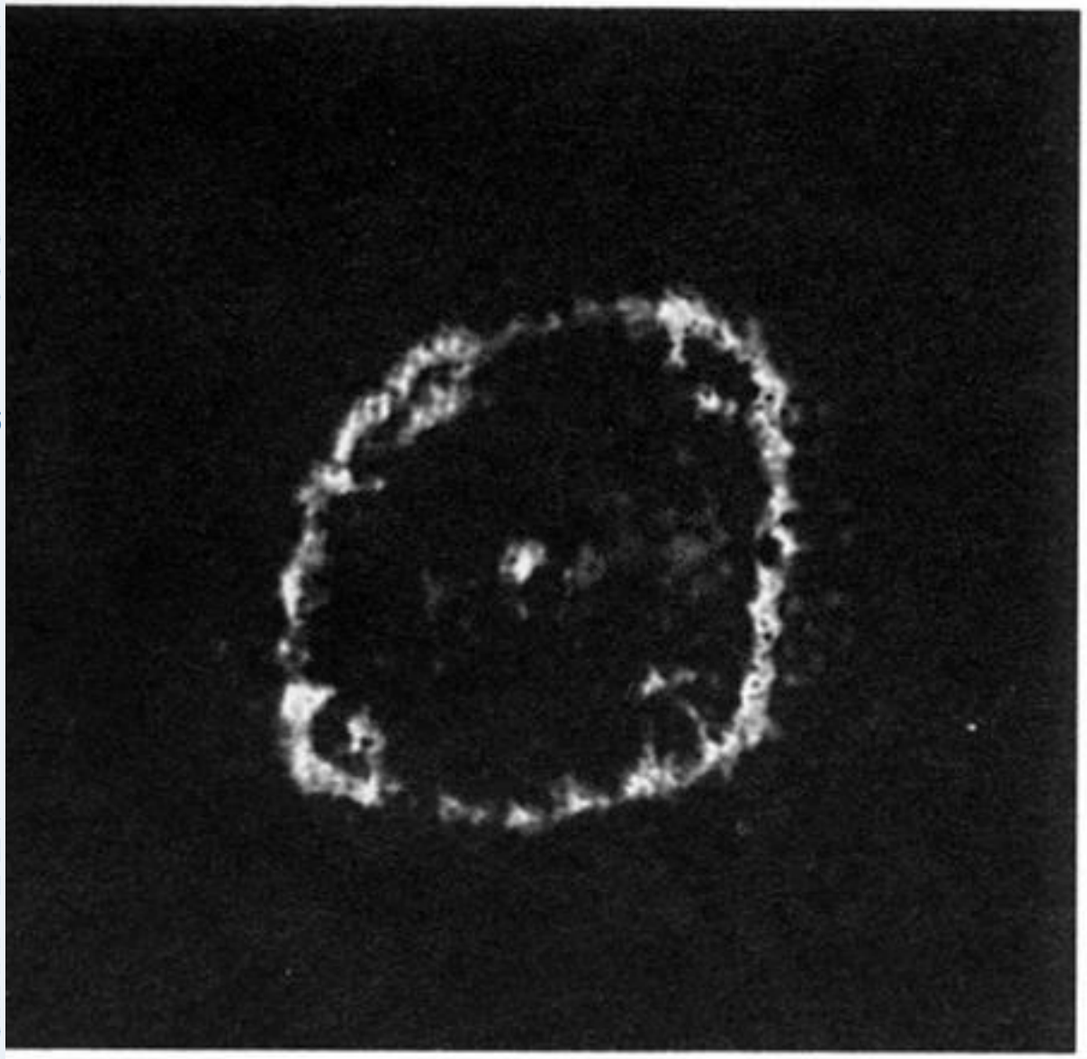

gure 3. 256 × 256 NMR image of a geranium stem. The in-plane resolution is 6.5 μm and the slice ickness is 100 μm.

Figure 4

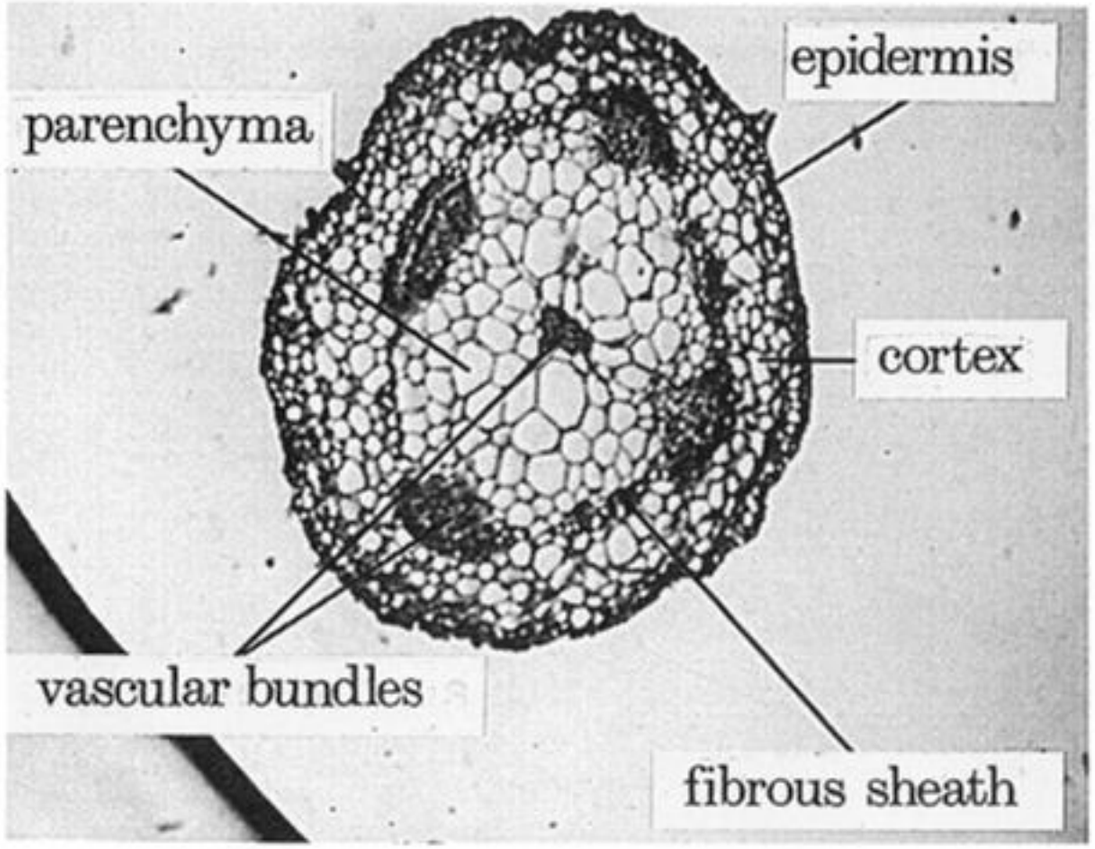

gure 4. Annotated optical micrograph of a section of the same geranium stem as seen in figure 3.

Figure 5

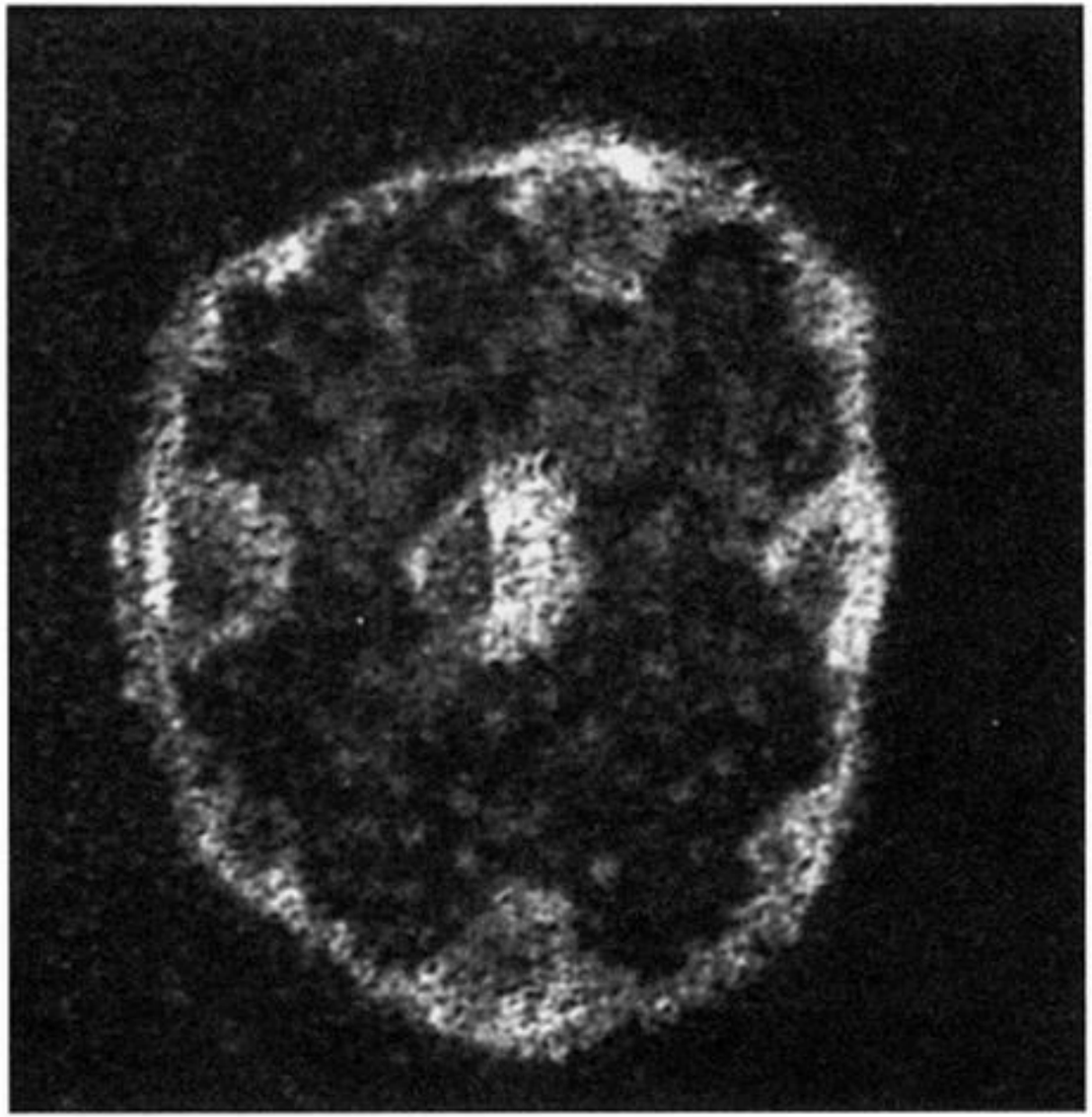

Figure 6

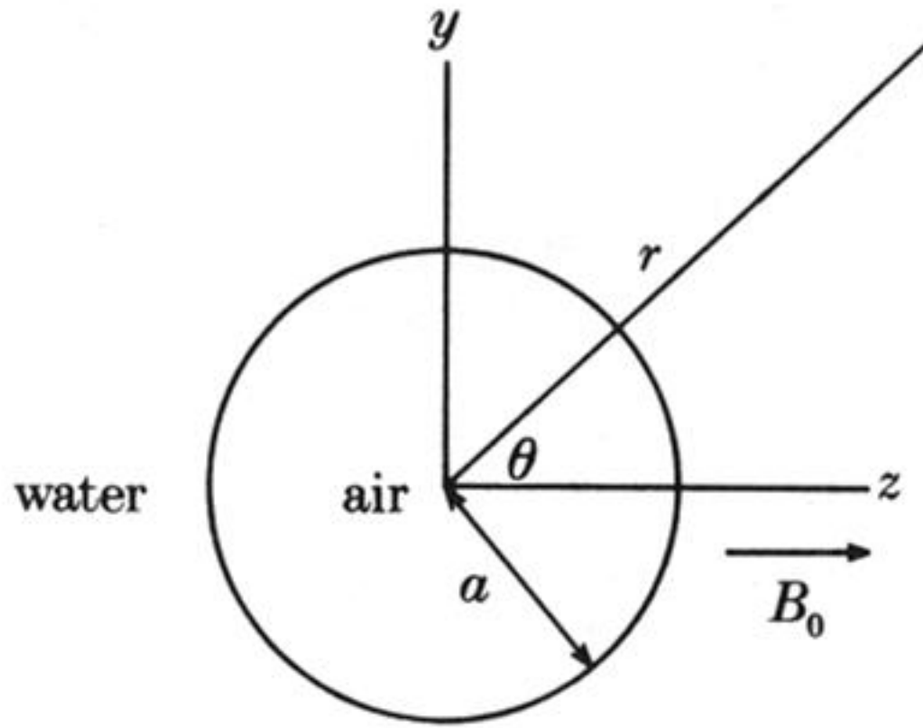

gure 5. NMR image of a geranium stem with an in-plane resolution of 4.5 μm and slice thickness
)0 μm.

gure 6. Geometry of a simple model of the intercellular air spaces.

PHILOSOPHICAL TRANSACTIONS OF THE ROYAL SOCIETY A MATHEMATICAL, PHYSICAL & ENGINEERING SCIENCES

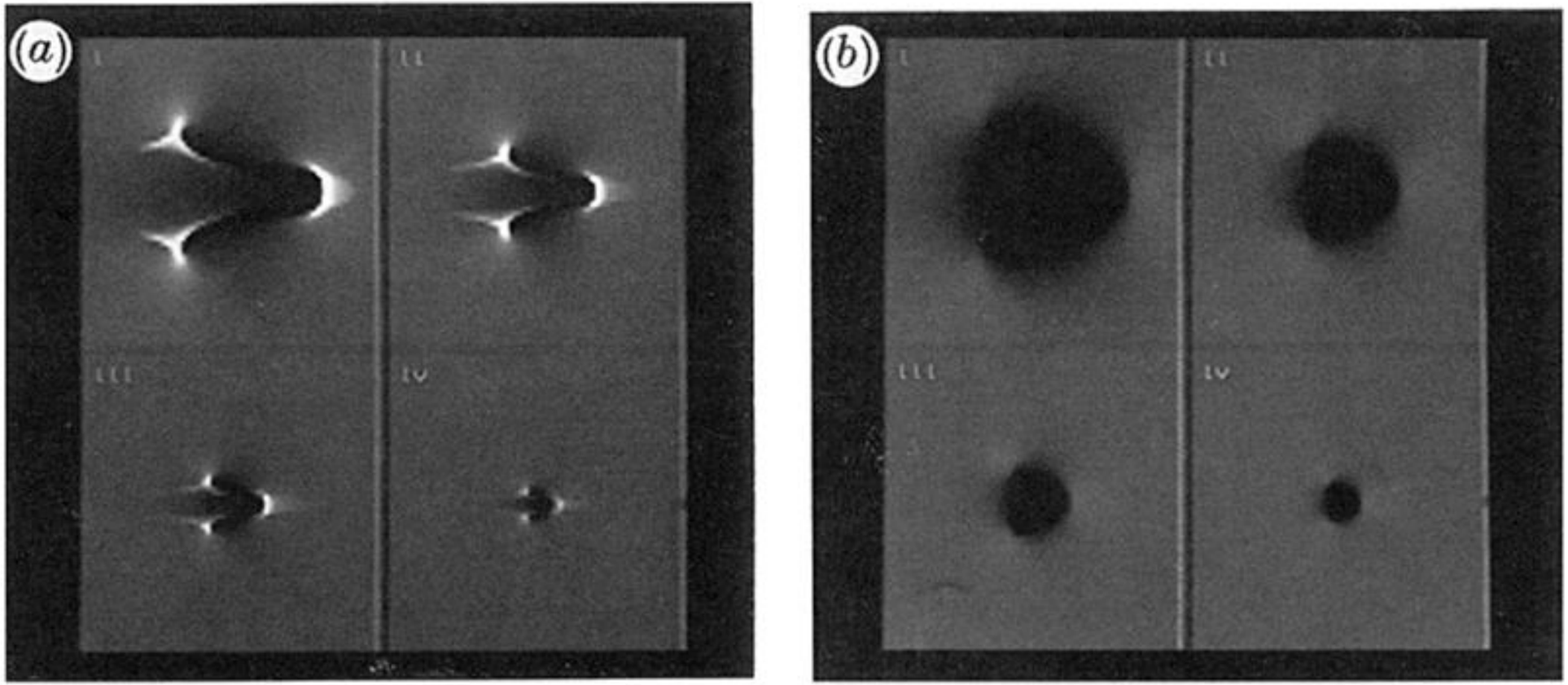

gure 7. Simulated NMR images of air cavities in water. The resolution is 6 μm, the gradient rength is 0.5 T m^{-1} and $\tau = 5.5$ ms. The cavity diameters are (i) 100 μm, (ii) 50 μm, (iii) 25 μm and) 10 μm. In (*a*) only the distorting effect of the extra field ΔB_0 is included. In (*b*) the effect of ffusion in the gradient G_s is also incorporated.

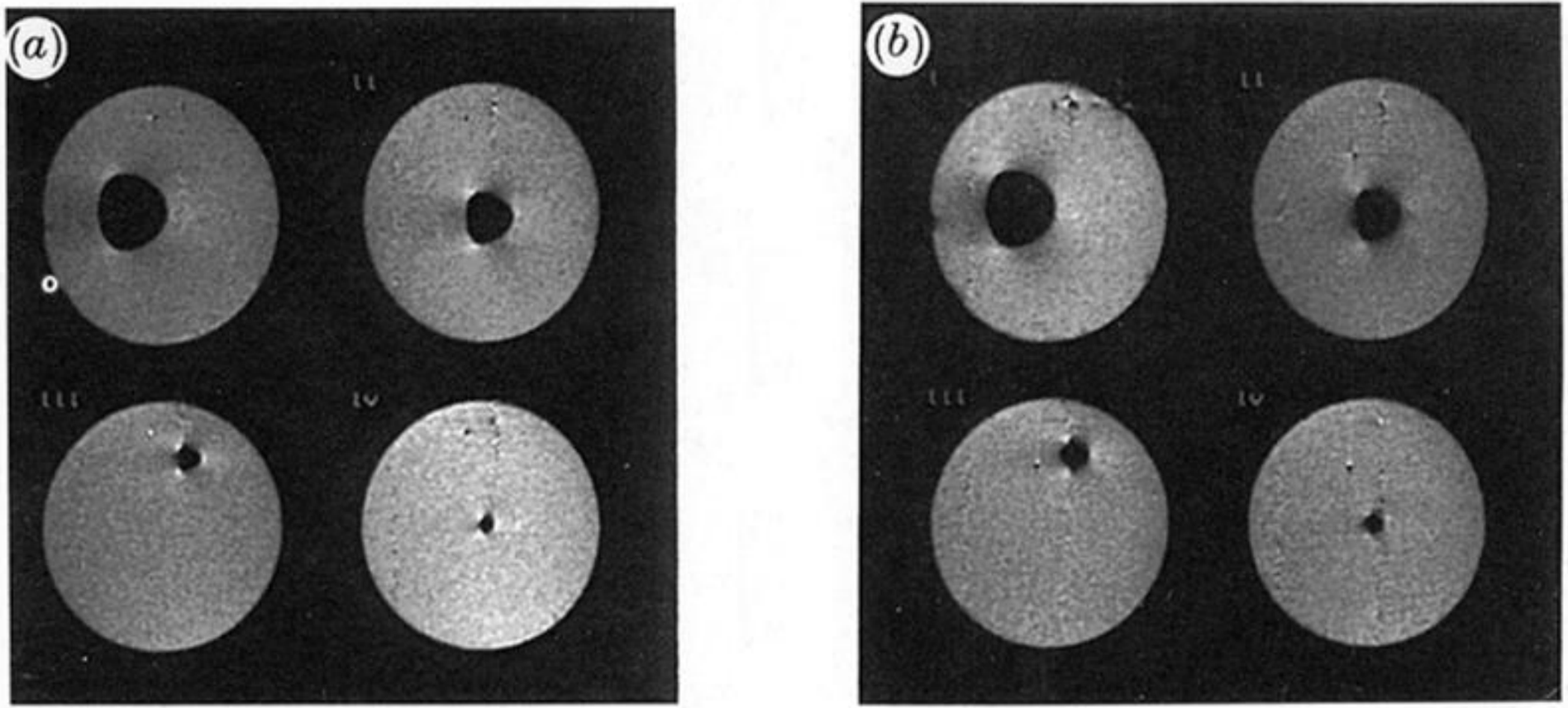

gure 8. 30 μm resolution images of glass fibres in water in a tube of diameter 3 mm. The fibre ameters are (i) 700 μm, (ii) 400 μm, (iii) 200 μm, and (iv) 100 μm. The gradient strength used was 0 mT m^{-1} and the bandwidth 20 kHz. In (*a*) $\tau = 5.5$ ms and in (*b*) $\tau = 15$ ms.

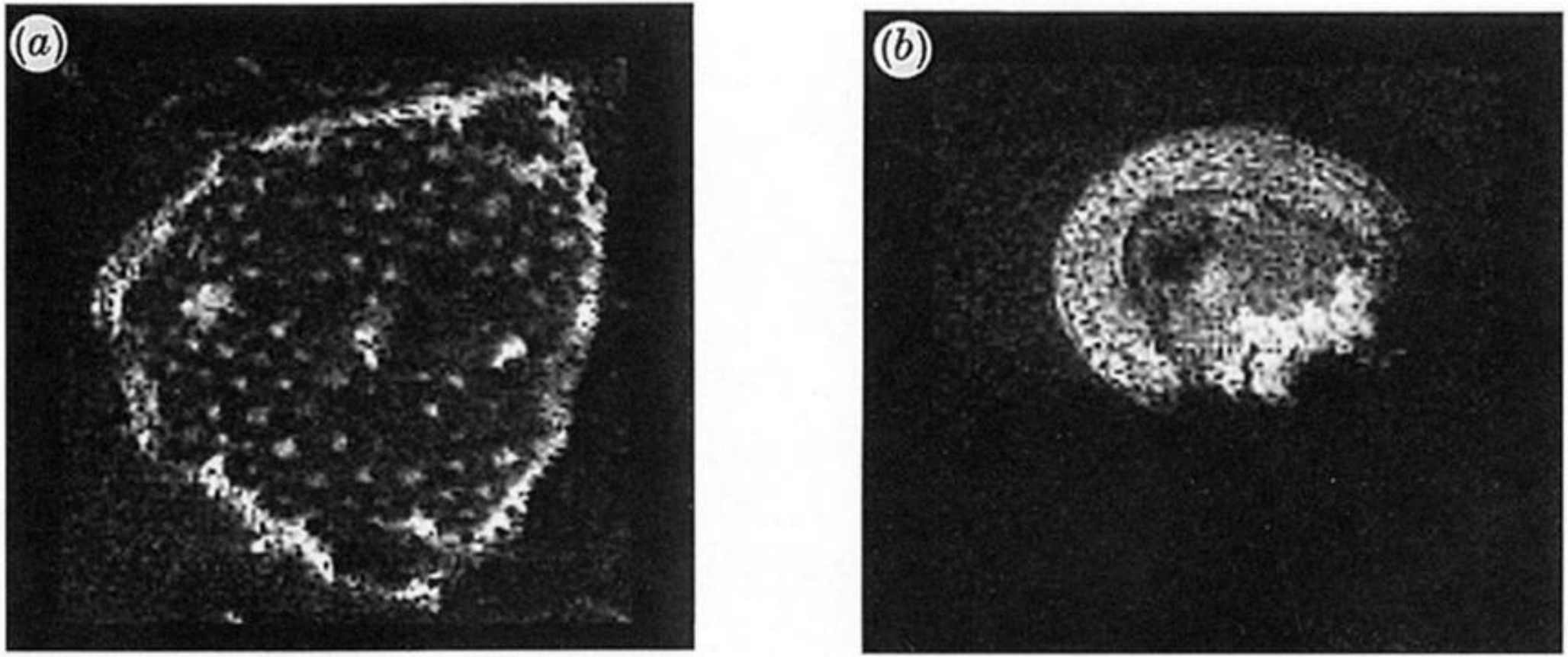

igure 9. (*a*) 7.5 μm resolution NMR image of an intact geranium stem. (*b*) One quarter of the same stem after sectioning and soaking in water for 15 min.

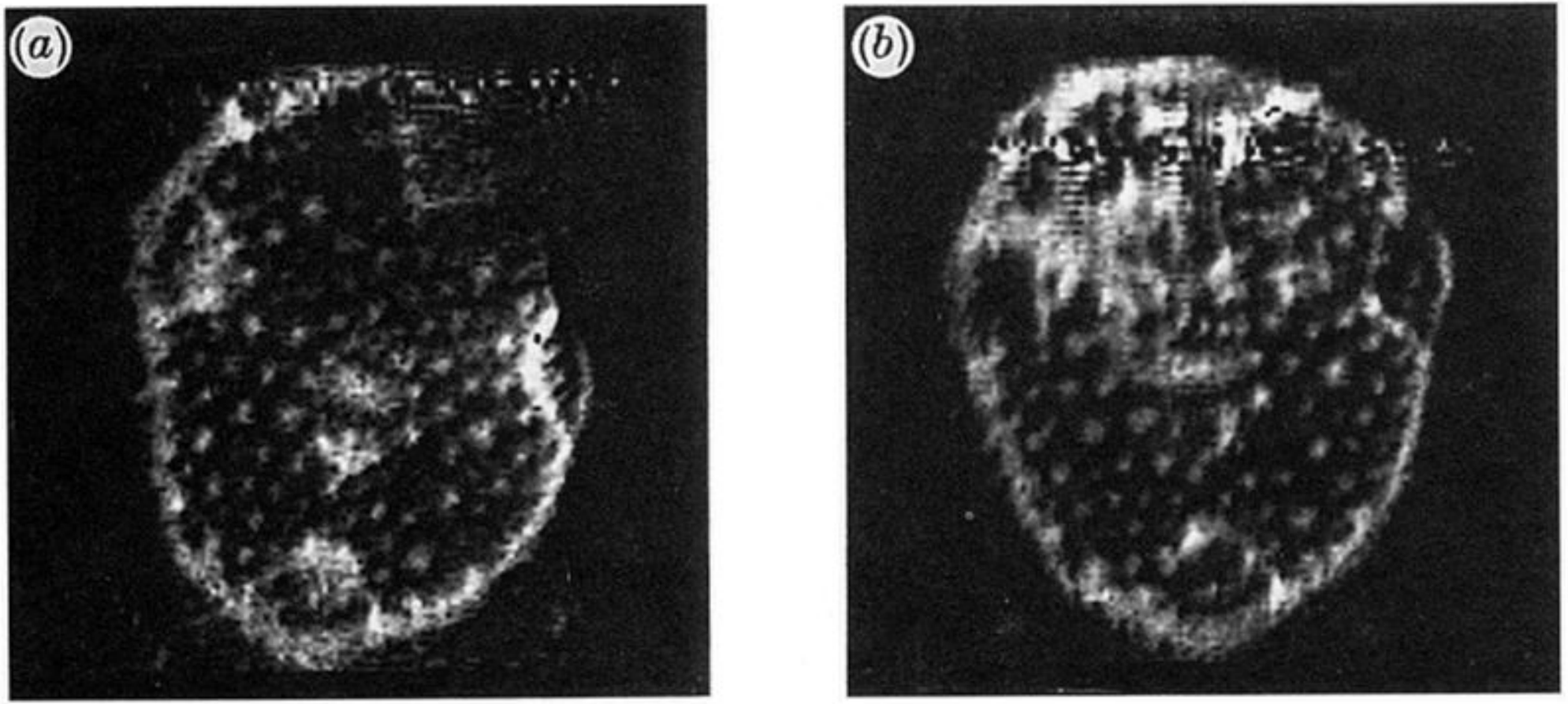

gure 10. 7.5 μm resolution NMR image of a geranium stem before (*a*) and after (*b*) bruising.

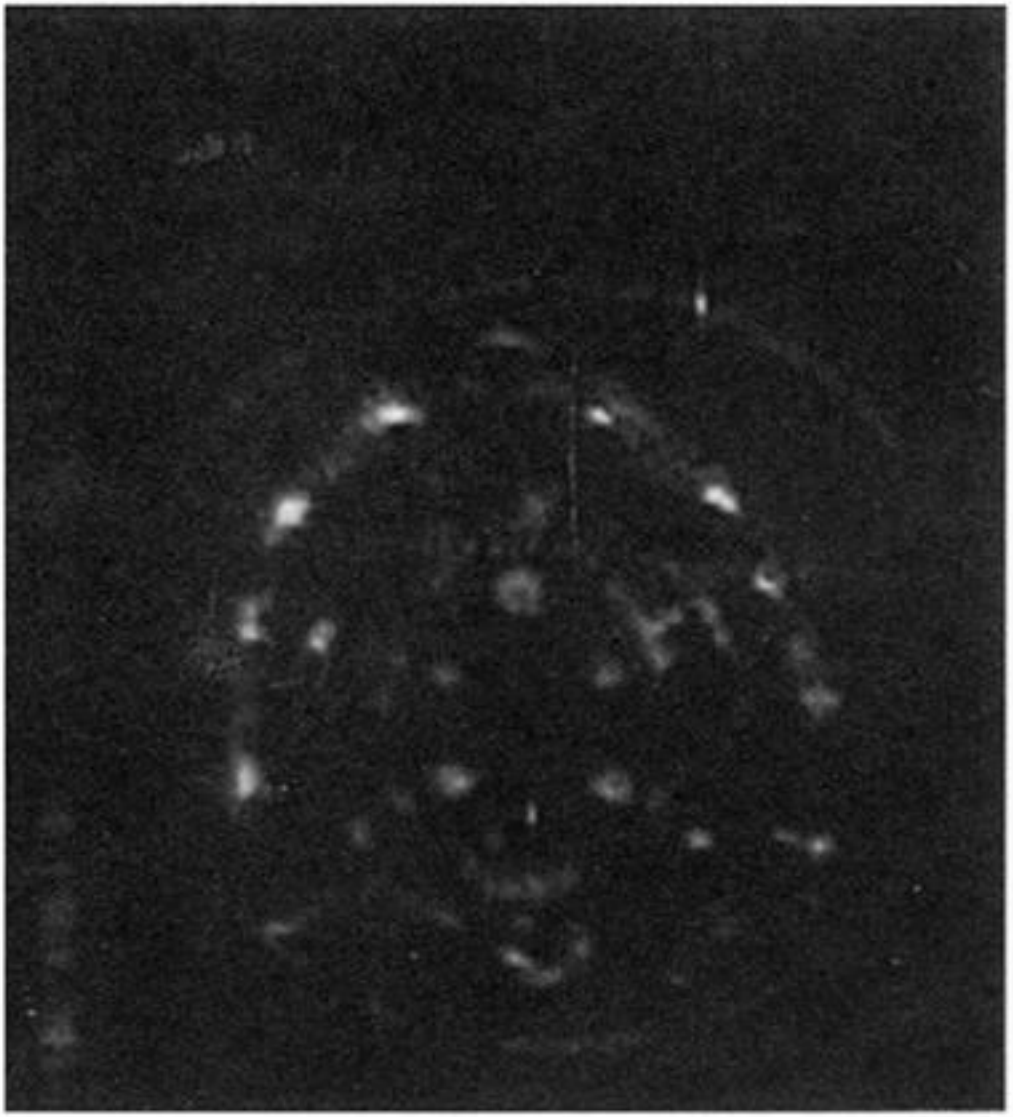

gure 11. 10 μm resolution NMR image of a grass stem.

PHILOSOPHICAL TRANSACTIONS OF THE SOCI